Carbohydrate Polymers 157 (2017) 65–71

Contents lists available at ScienceDirect

Carbohydrate Polymers

journal homepage: www.elsevier.com/locate/carbpol

Deciphering the potential of guar gum/Ag-Cu nanocomposite films as an active food packaging material

Yasir Ali Arfat, Mohammed Ejaz, Harsha Jacob, Jasim Ahmed *

Food and Nutrition Program, Environment & Life Sciences Research Center, Kuwait Institute for Scientific Research, P.O. Box 24885, Safat-13109, Kuwait

ARTICLE INFO

Article history:
Received 15 July 2016
Received in revised form 29 August 2016
Accepted 22 September 2016

Keywords:
Guar gum film
Ag-Cu bimetallic nanoparticles
Bionanocomposite material
Mechanical properties
Differential scanning calorimetry
Antimicrobial packaging

ABSTRACT

Guar gum (GG) based nanocomposite (NC) films were prepared by incorporating silver-copper alloy nanoparticles (Ag-Cu NPs) through solution casting method. Effect of NP loadings (0.5–2%) on the thermo-mechanical, optical, spectral, oxygen barrier and antimicrobial properties of the GG/Ag-Cu NC films were investigated. Tensile testing showed an improvement in the mechanical strength, and a decrease in elongation at break for all NP loadings. NP incorporation into GG films showed a marked influence on the color values. The NC films showed excellent UV, light and oxygen barrier capability. Thermal properties of the NC films were improved as evidenced from the differential scanning calorimetry and the thermal conductivity data. NC films became rough and coarse over neat GG film as visualized through the scanning electron microscopy. A strong antibacterial activity was exhibited by NC films against both Gram-positive and Gram-negative bacteria, and therefore, the film could be considered as an active food packaging.

1. Introduction

Packaging materials are mostly produced from petroleum-based polymers, which are non-biodegradable and have the adverse impact on the environment (Arfat, Benjakul, Prodpran, & Osako, 2014; Jamshidian, Tehrany, Imran, Jacquot, & Desobry, 2010; Krochta, & De Mulder-Johnston, 1997). In recent years, a considerable attention has been shifted from petroleum-based polymeric materials towards renewable and biodegradable natural polymers. Biodegradable polymers are obtained from various natural resources such as starch, cellulose, and protein and have several advantages including biocompatibility, edibility, and renewability (Banegas, Zornio, Borges, Porto, & Soldi, 2013; Rhim & Ng, 2007; Vroman & Tighzert, 2009).

The utilization of natural polysaccharides in food packaging has been a subject of intense investigation because of their biocompatibility and biodegradability (Cerqueira, Souza, Teixeira, & Vicente, 2012; Coma, 2013). Polysaccharides are long-chain polymers formed from mono- or disaccharide repeating units joined together by glycosidic bonds. A variety of polysaccharides like starch, chitosan, carrageenan, and galactomannans have been investigated for potential use as edible food packaging for their low cost, abundant supply and desirable functionalities (Rhim & Ng, 2007; Vroman & Tighzert, 2009). Among these, guar gum (GG) could be a prospective candidate due to its high molecular weight, long polymeric chain, and wide accessibility as compared to other biopolymers (Banegas et al., 2013; Saberi et al., 2016). GG is a hetropolysaccharide of a mannose [(1-4)-linked β-D-mannopyranose] backbone with galactose side groups [(1-6)-linked α-D-galactopyranose] and is extracted from the endosperm of an annual legume plant *Cyamopsis tetragonoloba* (Cunha, Castro, Rocha, de Paula, & Feitosa, 2005). GG is highly soluble in water and has good film forming ability. However, the applicability of GG in food packaging has been limited because of their inferior thermo-mechanical and barrier properties as compared to conventional polymer-based packaging materials (Banegas et al., 2013; Saurabh et al., 2015; Saurabh, Gupta, Variyar, & Sharma, 2016).

Nanoparticles, in general, offer enormous advantages over microparticles because of their large specific surface area and aspect ratio, excellent interfacial interactions on polymer branches. Dispersion of nanoparticles in the polymer matrix improves the desired properties of parent polymer matrix including tensile strength, glass transition temperature, thermal degradation, and rheological properties (Mbhele et al., 2003). To impart thermo-mechanical and barrier properties into the brittle guar gum films nanoparticles could be introduced. The antimicrobial activities of Ag NPs seem to be significantly higher than other metal NPs (Ag > Cu > Au > Zn > Fe) (Li et al., 2011). Additionally, bimetallic NPs such as Ag-Cu have superior optical, interfacial, catalytic and antimicrobial properties over single metallic NP when incorporated

* Corresponding author.
E-mail addresses: jaahmed@kisr.edu.kw, jahmed2k@yahoo.com (J. Ahmed).

http://dx.doi.org/10.1016/j.carbpol.2016.09.069
0144-8617/

in food packaging (Tan & Cheong, 2013). (Ahmed, Hiremath, and Jacob, 2016a; Taner, Sayar, Yulug, & Suzer, 2011; Tan, & Cheong, 2013; Valodkar, Modi, Pal, & Thakore, 2011; Zain, Stapley, & Shama, 2014). Apart from numerous benefits associated with the use of metal NPs, serious concerns related to the migration or leaching of NPs from nanocoated food packaging surface into food and their potential human toxicity once consumed have been reported (Cushen, Kerry, Morris, Cruz-Romero, & Cummins, 2013; Hannon et al., 2016). Few studies have reported the migration potential of NPs from food contact materials (FCMs) (Hannon, Kerry, Cruz-Romero, Morris, & Cummins, 2015a; Hannon et al., 2015b). Emamifar, Kadivar, Shahedi, and Soleimanian Zad (2011) detected release of silver and zinc at very low levels (after 112 days storage at 4 °C) when orange juice was packed in LDPE films containing either 5% AgNP on TiO2 powder or 1% ZnO nanoparticles. From a food safety point of view, a knowledge of NP migration from NP packaging to food sample and its quantitative assessment, and above all determination of corresponding potential human exposure is highly desired.

Therefore, the objectives of the work were to develop GG/Ag-Cu nanocomposite films, and characterize their mechanical, thermal, structural and morphological properties. Finally, the antimicrobial properties of the developed films were tested against Gram-positive *Listeria monocytogenes* and Gram-negative *Salmonella enterica* sv *typhimurium*, respectively. This information could be useful for commercial development of GG/Ag-Cu nanocomposites films, and their possible applications in active food packaging.

2. Materials and methods

2.1. Chemicals

Guar gum (GG) and Ag-Cu nanoparticles (particle size: <100 nm) were purchased from Sigma-Aldrich (St. Louis, MO, USA). Lyfo Disk pellets® of *Listeria monocytogenes* (ATCC 19114) strain was purchased from MediMark Europe (Grenoble, CEDEX, France). Culti-loops® of *Salmonella enterica* sv *typhimurium* (ATCC 14028) was obtained from Remel Europe Ltd. (Dartford, Kent, UK). Brain heart infusion agar (BHIA) was procured from Conda Laboratories (Torrejón de Ardoz, MD, Spain). Muller Hinton agar (MHA) and Tryptic soya broth (TSB) were purchased from TM Media (Bhiwadi, India). All materials were used as such except GG which purified before use.

2.2. Preparation of GG/Ag-Cu nanocomposite film

Ag-Cu NPs (0, 0.5, 1 and 2% of GG, w/w) were mixed with distilled water and the suspensions were stirred for 5 min, and homogenized thereafter, for a min at 5000 rpm (IKA Labortechnik homogenizer, Selangor, Malaysia). For the preparation of GG/Ag-Cu nanocomposite films, purified GG was added to different dilutions of dispersed Ag-Cu NPs suspension to make 1% w/v aqueous solution (150 mL). This was followed by the addition of glycerol at concentrations of 30% (w/w) of GG as a plasticizer. To ensure the mixing and uniform distribution of GG and Ag-Cu NPs, the suspensions were sonicated for 30 min (Branson Ultrasonics, CT, USA). The resultant mixtures were referred to as a film-forming suspension (FFS) which gently stirred for 2 h at room temperature to obtain a homogenous suspension. Prior to casting, FFS samples were degassed for 10 min using the sonicating bath.

To prepare the film, 50 mL of solution was poured and spread evenly onto surface of glass plate (8 cm × 8 cm), having removable boundary of insulating tape. For drying, plates were then kept in oven for 8 h at 80 °C. Dried nanocomposite films were conditioned in an environmental chamber (Binder GmbH, Tuttlingen, Germany) at 25 ± 0.5 °C and 50 ± 5% relative humidity (RH) for 3 days. Conditioned film samples were manually peeled off and subjected to analyses. For Fourier transform infrared (FTIR) spectroscopy, differential scanning calorimetry (DSC), and Scanning electron microscopy (SEM) analyses films were dried in a desiccator containing dried silica gel for 2 weeks at room temperature (25–28 °C) to minimize the plasticization effect.

2.3. Characterization of films

2.3.1. Film thickness, mechanical properties and thermal conductivity

The thickness of films was measured using a digital handheld micrometer (Mitutoyo, Model MCD-1"PXF, Mituyoto Corp., Kawasaki-shi, Japan) with a precision of 0.001 mm. Eight random locations around each film sample were used for average thickness determination.

Tensile strength (TS) and elongation at break (EAB%) were measured using a Texture Analyzer TA.XT plus (Stable Micro Systems, UK) with a 50 N load cell equipped with tensile grips (A/TG model) as per the ASTM standard of D 882 (ASTM, 2001). Cross-head speed was 30 mm/min and grip separation was set at 30 mm. Tensile properties were evaluated in ten samples from each type of film.

Thermal conductivity, diffusivity and specific heat were measured by a Hot Disk TPS 500 Thermal Conductivity meter (Hot Disk, Gothenburg, Sweden), and the data were obtained directly from the instrument software. The method is based on Transient Plane Source method.

2.3.2. Color and optical properties

The color of the films was measured by a CIE colorimeter (Hunter associates laboratory, Inc., Reston, VA, U.S.A.) and was expressed as L^* (lightness), a^* (redness and greenness), b^* (yellowness and blueness) and ΔE^* (total difference in color) values. Color values were reported by taking an average of six evaluations from each film sample. The light transmittance at the ultraviolet and visible range (200–800 nm) and transparency values of films was measured using a UV–vis spectrophotometer (Shimadzu UV-1800, Kyoto, Japan).

2.3.3. Oxygen permeability

The oxygen transmission rate (OTR) was measured at 23 °C and 50% RH by an Extra-Solution Perme O_2 instrument (Capannori, LU, Italy) according to the American Society of Testing and Materials Standard Method D 3985 (ASTM 1995). Films with an open testing area of 50 cm^2 were placed into the test cell and exposed to 99% N_2 + 1% H_2 flow on one side and pure oxygen flow on the other. The oxygen permeability (OP) was calculated by dividing the OTR by the oxygen partial pressure difference between the sides of the film (1 atm) and multiplying by the average film thickness.

2.3.4. Fourier transform infrared (FTIR) spectroscopy

The FTIR spectra of film samples were determined in the wave number of 500–4000 cm^{-1} using a Nicolet iS5 FT-IR Spectrometer (Thermo Scientific, Madison, WI, USA). Film samples were placed on the surface in contact with attenuated total reflectance (ATR) on a multi-bounce plate of Zn-Se crystal at 25 °C. Each spectrum collected from an average of 32 scans at a resolution of 4 cm^{-1} was taken against a background recorded from the air spectrum at 25 °C. The results were reported as mean values.

2.3.5. Differential scanning calorimetry (DSC)

DSC thermograms of the films were determined using a differential scanning calorimeter (TA Q2000, USA) under a nitrogen atmosphere. Film samples (≈10 mg) were weighed into aluminum pans, hermetically sealed, and scanned over the temperature range

Table 1
Thickness, tensile strength, elongation at break and thermal property of GG/Ag-Cu nanocomposite films.

Film samples	Thickness (mm)	Tensile strength (MPa)	EAB (%)	Thermal conductivity W/mK	Thermal diffusivity mm^2/s	Specific Heat Mj/m^3 K
Control GG	0.048 ± 0.001^b	15.4 ± 2.1^b	30.4 ± 2.8^a	0.082 ± 0.005^a	0.088 ± 0.005^a	0.937 ± 0.003^a
GG/0.5% Ag-Cu NP	0.050 ± 0.002^b	16.1 ± 3.0^b	28.7 ± 2.4^a	ND	ND	ND
GG/1% Ag-Cu NP	0.054 ± 0.003^a	20.2 ± 2.8^{ab}	26.5 ± 2.1^{ab}	0.181 ± 0.004^b	0.232 ± 0.023^b	0.794 ± 0.042^b
GG/2% Ag-Cu NP	0.057 ± 0.002^a	23.7 ± 3.2^a	23.5 ± 1.1^b	0.475 ± 0.069^c	1.947 ± 0.092^c	0.179 ± 0.068^c

Values are given as mean ± SD (n = 3). Different superscript letters in the same column indicates significant differences ($p < 0.05$).

Table 2
Instrumental color values of GG/Ag-Cu nanocomposite films.

Film samples	Color parameters			Color difference
	L^*	a^*	b^*	ΔE^*
Control GG	90.54 ± 1.21^a	-1.87 ± 0.11^d	2.41 ± 0.21^d	3.65 ± 0.42^d
GG/0.5% Ag-Cu NP	58.58 ± 1.1^b	0.53 ± 0.06^c	10.92 ± 0.15^c	36.55 ± 1.44^c
GG/1% Ag-Cu NP	43.5 ± 0.73^c	1.64 ± 0.04^b	13.54 ± 0.24^b	51.82 ± 2.13^b
GG/2% Ag-Cu NP	37.19 ± 0.6^d	1.79 ± 0.03^a	15.43 ± 0.31^a	58.40 ± 1.86^a

Values are given as mean ± SD (n = 3). Different superscript letters in the same column indicate significant differences ($p < 0.05$).

of −60 °C to 400 °C with a heating rate of 10 °C/ min. Film samples were equilibrated at −60 °C and isothermed for 2 min; heated to 400 °C at 10 °C/min and isothermed for 2 min; cooled to −60 °C at 10 °C/min. The empty aluminum pan was used as a reference.

2.3.6. Scanning electron microscopy (SEM)

Surface morphology of film samples were visualized using a scanning electron microscope (SEM) (Quanta400, FEI, Tokyo, Japan) at an accelerating voltage of 10 kV. Prior to surface morphology visualization, the film samples were fixed on brass stub and sputtered with platinum in order to make the sample conductive, and photographs were taken at a magnification of 250×.

2.3.7. Antibacterial activity

The antibacterial activities of GG/Ag-Cu films were evaluated against the growth of two common food-borne bacterial pathogens, *Listeria monocytogenes* (Gram positive) and *Salmonella enterica* sv *typhimurium* (Gram negative). TSB cultures were used to assess the antibacterial activity of the different films according to the method of Teixeira et al. (2014) with some modifications. Briefly, two pieces of circular film discs (20 mm diameter) were sterilized under ultraviolet light and immersed in a test tube containing 10 mL TSB. The TSB was inoculated with 0.1 mL (~10^8 CFU/mL) inoculum and incubated at room temperature (25 °C) under mild shaking (200 rpm) conditions. One milliliter of the inoculated medium was sampled after 24 h. Specimens were serially diluted with sterile buffered peptone water and then spread plated onto BHI agar. Plates were incubated at 37 °C for 24 h and the colony-forming units (CFU) were counted. Film samples without Ag-Cu NPs served as control.

2.4. Statistical analysis

Experiments were run in triplicate using different three lots of samples. Data were subjected to analysis of variance (ANOVA) and mean comparisons were carried out by Duncan's multiple range test (Steel & Torrie, 1980). Statistical analysis was performed using the Statistical Package for Social Science (SPSS 17.0 for windows, SPSS Inc., Chicago, IL, U.S.A.).

3. Results and discussion

3.1. Thickness of nanocomposite films

Thickness of GG/Ag-Cu NC films is presented in Table 1. The thickness of the GG film increased linearly with increasing the loading concentration of NP (Eq. (1)). The thickness of the control film was 0.048 mm which increased to 0.057 mm with addition of 2% NPs. Such increase was as expected because of the incorporation of Ag-Cu NPs, which increased the solid contents in the film. A similar increase in thickness has been reported for various biopolymer nanocomposite films (Arfat et al., 2016; Shankar, Teng, Li, & Rhim, 2015).

$$Thickness = 0.0046NP + 0.0482 \left(R^2 = 0.96\right) \quad (1)$$

3.2. Mechanical properties

Mechanical properties of GG/Ag-Cu nanocomposite films are presented in Table 1. The tensile strength (TS) of the composite films increased from 15.4 to 23.7 MPa when the loading of NP was increased from 0 to 2% (w/w), and the elongation at break (EAB) decreased from 30.4 to 23.5% at similar condition. TS increased linearly with increasing the NP concentration (Eq. (2)), whereas the EAB of the nanocomposites exhibited a linear decrease at similar condition (Eq. (2)) ($p < 0.05$). Incorporation of NPs to composite produced a stiffer material with less flexibility which confirmed the reinforcing effect of the Ag-Cu in the GG matrix. A similar observation has been reported by various authors for bionanocomposites (Alamsi, Ghanbarzadeh, & Entezami, 2010; Ahmed et al., 2016b; de Moura et al., 2009; Rouhi, Mahmud, Naderi, Ooi, & Mahmood, 2013). Furthermore, the chain mobility of the GG became restricted in NC due to presence of Ag-Cu NPs, and therefore, the TS increased significantly (Ahmed et al., 2016b).

$$TS = 4.42NP + 14.98 \left(R^2 = 0.95\right) \quad (2)$$

$$EAB = -3.48NP + 30.32 \left(R^2 = 0.99\right) \quad (3)$$

Where all these equations are valid only the NP concentrations of 0–2% only.

3.3. Thermal conductivity

The thermal conductivity (K) of the GG film was 0.082 W/m K, and it increased abruptly to 0.475 W/m. with 2% Ag-Cu NP loading (Table 1). A similar increasing trend was also observed for the thermal diffusivity (0.088–1.947 mm^2/s), whereas the specific heat decreased (0.937–0.179 MJ/m^3 K) with increasing loading concentration. Such significant changes in thermal properties have been influenced by the addition of metal NPs into GG matrix.

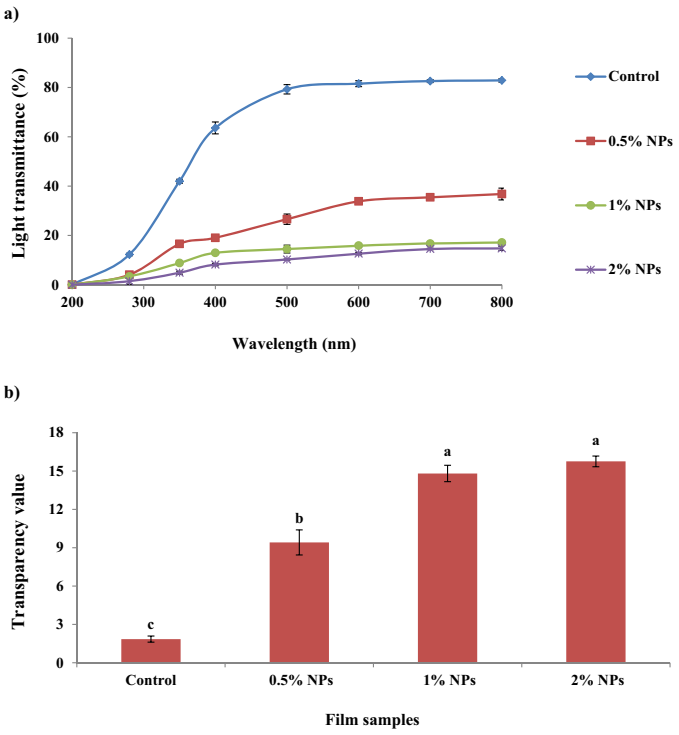

Fig. 1. Light transmittance (a) and transparency (b) of GG/Ag-Cu nanocomposite films. Bars represent the standard deviation (n = 3). Different lowercase letters on the bars indicate significant differences ($p < 0.05$).

3.4. Color

Addition of Ag-Cu NPs into GG films exhibited a significant effect on the instrumental color values L^*, a^* and b^* ($p < 0.05$) (Table 2). The lightness, L* values decreased significantly from 90.5 to 37.2, and the film transformed to grey or partially black. Both red (a*) and yellowness (b*) values of the NC films also improved with the NP loading concentration. These observations were close in agreement with Rhim, Wang, and Hong (2013); they reported that an increasing amount of Ag NPs markedly dropped the L* value, while a^* and b^* values dropped for agar/Ag nanocomposite films. Such change in the color values was mainly attributed by the characteristic surface plasmon resonance (SPR) of silver and copper NPs (Varshney, Bhadauria, Gaur and Pasricha, 2010; Zeng, Rong, Zhang, Lianm, & Zeng, 2001).

3.5. Optical properties

Transmittance of films was greatly influenced by the addition of Ag-Cu NPs. The control film was a transparent one with high transmittance value at 600 nm (81.54%), and had the modest UV barrier property as indicated by the low transmittance value at 280 nm (12.25%) (Fig. 1a).The percent transmittance (%T) of films in both UV and visible wavelength decreased with increasing NP concentration from 0.5 to 2% ($p < 0.05$). The%T of control GG films decreased significantly with NPs incorporation at 280 nm. The control GG film at visible region showed high transmittance values (Fig. 1a), which indicating that the control GG film is very clear and transparent. The%T of GG film at 600 nm decreased to 12.63 after incorporation of 2% Ag-Cu NPs. It clearly demonstrates that the NPs play an important role in blocking both UV and visible light in the films due to the opaqueness of NPs and hindrance of light passage or light scattering by the NPs dispersed in the film matrix (Arfat et al., 2016). The developed nanocomposite films with excellent UV and light barrier capability could be used as packaging for oxidation prone food materials. Similar change in light transmittance has been observed in gelatin/silver nanocomposite films (Kanmani & Rhim, 2014).

The transparency value of the film increased as the NP loading increased from 0.5 to 2% ($p < 0.05$) indicating a decrease in the transparency of resulting films (Fig. 1b). This was attributed to the opaqueness of Ag-Cu NPs, which was distributed throughout the films. Similar results were reported by Arfat et al. (2015) for fish protein isolate/fish skin gelatin/ZnO nanocomposite films.

3.6. Oxygen permeability

Neat guar gum and GG/2% Ag-Cu NC films were determined to have oxygen permeability (OP) values of 7.06 ± 1.1 and 3.96 ± 0.55 (cc mm/m^2 d atm), respectively. OP of GG dropped with increased addition of NP in the GG polymer matrix. The OP of the GG/2% Ag-Cu was reduced by 56.1% because of the high aspect ratio of NP and its distribution throughout the film matrix. Additionally, it acts as impermeable obstacles in the path of the diffusion process. In a dispersed state, NPs are believed to increase the oxygen barrier properties by creating tortuous path that retards the progress of gas and vapor molecules through the film material (Petersson & Oksman, 2006). Thus, an improvement of the oxygen barrier properties of nanocomposites can be attributed to the increment in tortuosity and also associated with the decrease in free volume available for gas transport (Bhattacharya, Biswas, & Bhowmick, 2011).

3.7. FTIR spectroscopy

FTIR spectra of the control and GG/Ag-Cu NC films are presented in Fig. 2. The spectrum of control GG film exhibited broad peak around 3317 cm^{-1}, which is attributed to —OH stretching vibration of biopolymer and water involved in hydrogen bonding (Fringant, Tvaroska, Mazeau, Rinaudo, & Desbrieres, 1995; Mudgil, Barak, & Khatkar, 2012). The absorption bands in the 3000–2800 cm^{-1} region are ascribed to the C—H stretching of CH_2 group (Banegas et al., 2013). The peak appeared at 1651 cm^{-1} is due to the bending vibration of —OH group and associated water molecule (Mudgil et al., 2012). The peak at 1370 cm^{-1} is ascribed to symmetrical deformations of CH_2 group (Kačuráková, Ebringerova, Hirsch, Hromadkova, 1994). A small peak at 1147 and strong absorption peaks at 1020 cm^{-1} represent C—O—C asymmetric stretching vibration and stretching vibration of C—O(H), respectively (Banegas et al., 2013; Gong et al., 2011). The peaks appeared in the spectra between 800 and 1000 cm^{-1} represented the highly coupled C—C—O, C—OH and C—O—C stretching modes of polymer backbone (Kačuráková, Belton, Wilson, Hirsch, & Ebringerová, 1998; Mudgil et al., 2012).

FTIR spectrum of the NC did not show any additional peak attributed by bimetallic Ag–Cu NP. It indicates that there was no chemical bonding or interaction between GG matrix and Ag-Cu NPs. However, a minor shift in the wavenumber around 3300–2800 cm^{-1} has been observed. Similar results have been reported by Ahmed et al. (2016b) for PLA/Ag-Cu NC.

3.8. Thermal analysis

Fig. 3 illustrates the DSC curves for the neat GG and NC films where two endothermic and one exothermic peaks were detected. For the neat GG, endothermic peaks were traced at about 106 and 254 °C (Fig. 3a), and the exothermic peak was at about 305 °C (Fig. 3b). The first endotherm at 106 °C is believed to be associated with the glass transition temperature (T_g) of the polymer. A similar observation has been reported by several researchers for the neat GG (Gong et al., 2011; Kumar, De, & Mozumdar 2015), and they found a T_g value of 108 °C. The first peak temperature increased with increasing NP concentration, and the value equaled at 109

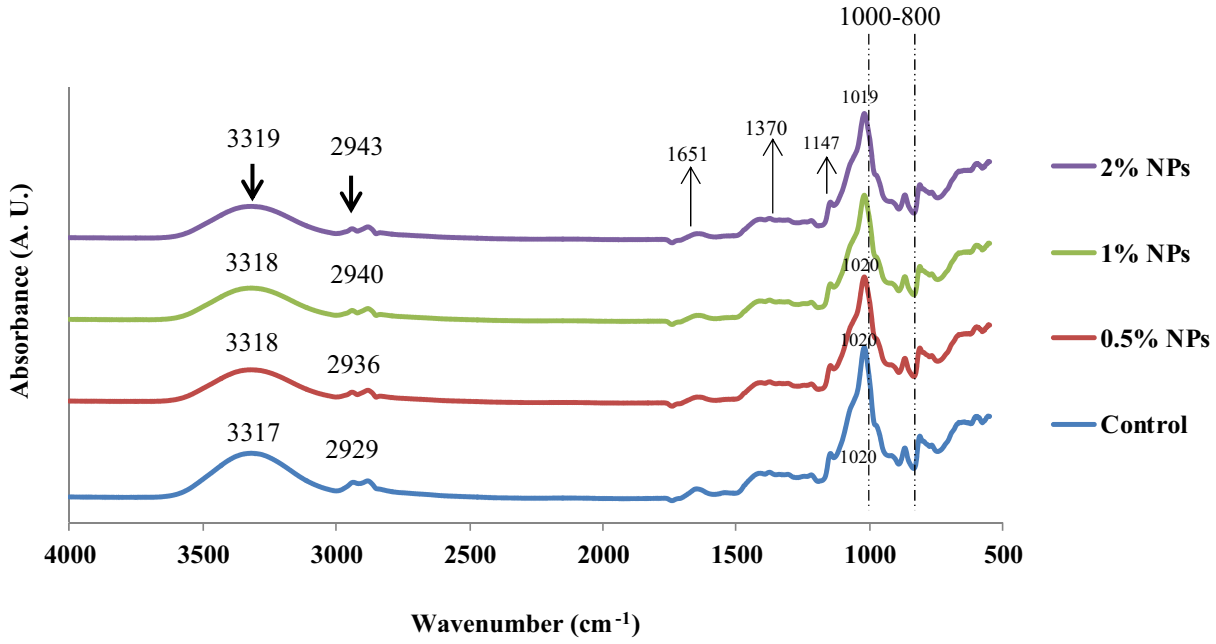

Fig. 2. ATR-FTIR spectra of control GG film and GG films incorporated with 0.5, 1 and 2% (w/w) Ag-Cu NPs.

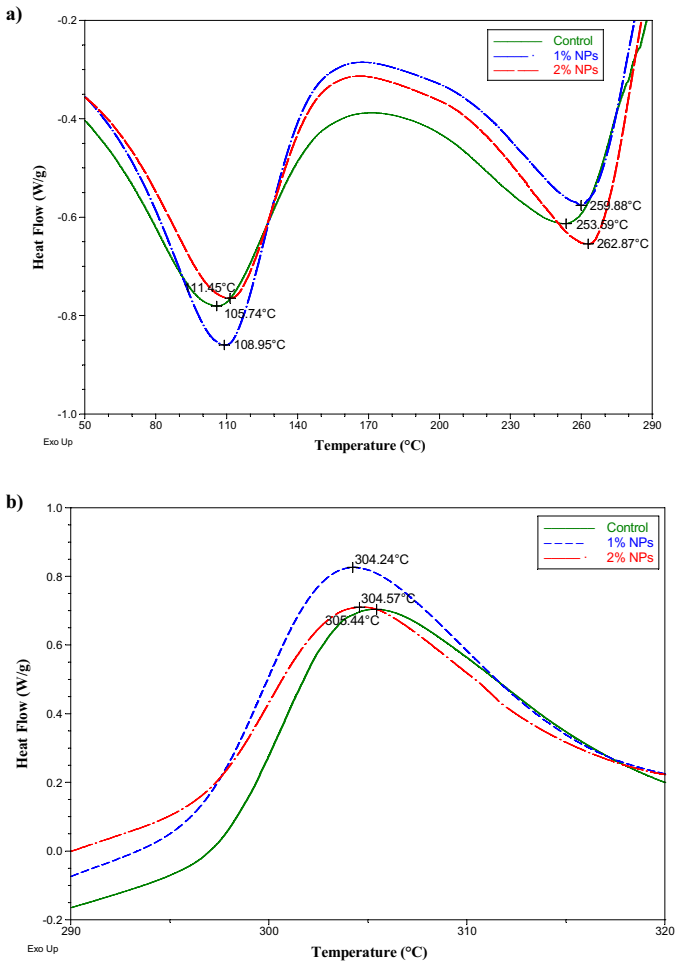

Fig. 3. DSC thermograms of control GG and GG nanocomposite films; (a) endothermic peaks and (b) exothermic peak temperature.

and 111 °C for 1 and 2% loading, respectively. This increase of T_g is due to the confinement of the GG chains adjacent to the NPs that prevent the segmental mobility of the biopolymer chains. Cacciotti, Fortunati, Puglia, Kenny, and Nanni (2014) found an increase in the T_g of an Ag incorporated biopolymer film loaded with 1% Ag NP. The second endotherm was increased from 254 °C to 260 and 263 °C after reinforcement with 1 and 2% NP, respectively. Mudgil, Barak, and Khatkar (2012) observed a similar value of 253 °C for the second endotherm of GG. This endotherm could be associated to the initiation of thermal degradation of the polymer due to cleavage of galactose and mannose units from GG backbone (Mudgil et al., 2012). The exothermic peak almost remained unaffected by incorporation of the NP as evidenced from Fig. 3b. Exothermic peak corresponds to continuing thermal and oxidative decomposition of the polymer, vaporization and elimination of volatile products (Ramos-Sanchez, Rey, Rodriguez, Martin-Gil, & Martin-Gil, 1988).

3.9. Scanning electron microscopy (SEM)

Surface morphology of control GG and GG/2% Ag-Cu nanocomposite films were observed by SEM and the results are shown in Fig. 4. The morphology of the neat film was smooth, homogeneous and compact, whereas the NP incorporation developed roughness in the film surface although the NPs were distributed uniformly on the GG matrix. A similar surface morphology was observed when ZnO NPs were reinforced into polylactide matrix to develop PLA/ZnO nanocomposite films (Ahmed et al., 2016b).

3.10. Antibacterial activity

Antimicrobial activity of control GG and GG/Ag-Cu NPs composite films was tested against Gram-positive (*L. monocytogenes*) and Gram-negative (*S. typhimurium*) food-borne pathogenic bacteria, and the results are presented in Fig. 5. GG/Ag-Cu nanocomposite films with loading concentration of 0.5–2% showed a distinct antimicrobial activity against both *L. monocytogenes* and *S. typhimurium* in a concentration dependent manner, nonetheless, the control GG film as expected did not exhibit any inhibitory action. The strong antimicrobial activity of Ag-Cu NPs and the

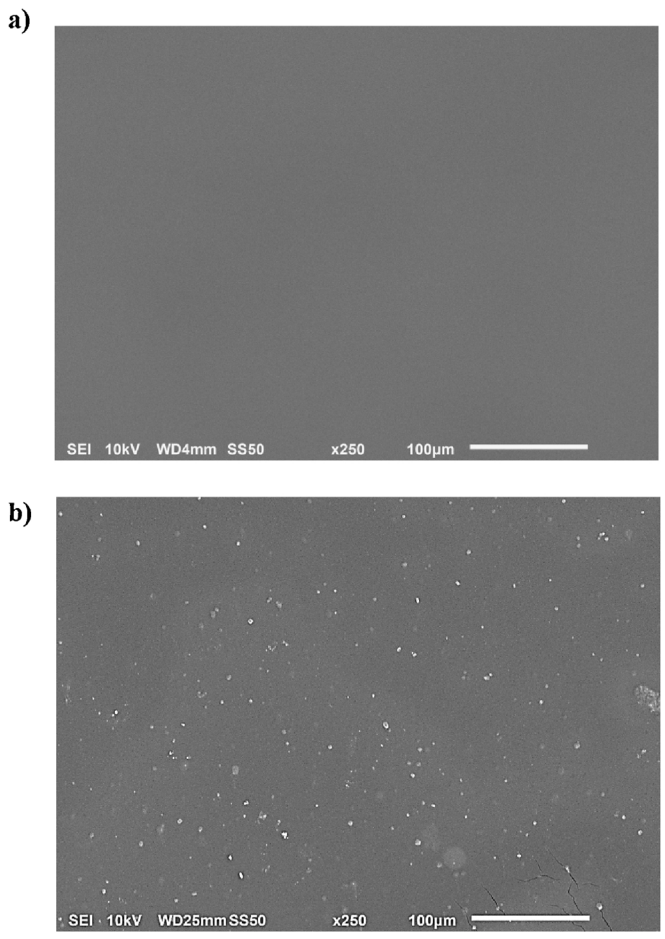

Fig. 4. Scanning electron surface micrographs of (a) control GG film and (b) GG film incorporated with 2% Ag-Cu NPs. Magnification ×250.

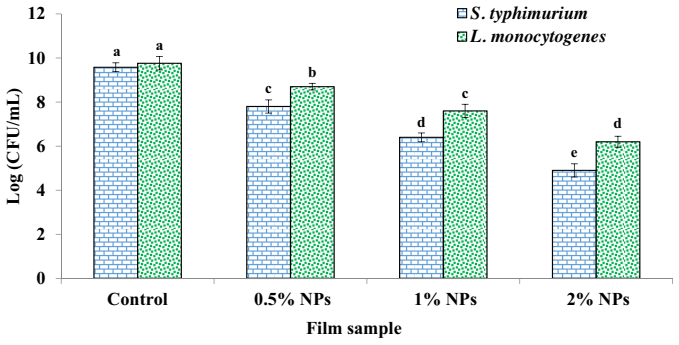

Fig. 5. Antibacterial activities of control GG and GG/Ag-Cu NPs films against *L. monocytogenes* and *S. typhimurium*. Bars represent the standard deviation (n = 3). Different lowercase letters on the bars indicate significant differences ($p < 0.05$).

mechanism of the action against the microorganisms could be associated with the release of silver and copper ions that could penetrate through the bacterial membrane and react with interior components that finally affect the viability of the cells. Ag NPs has been known to interact with sulfhydryl or disulfide groups of proteins, DNA and enzymes preventing DNA replication, and leading to cell death (Dizaj et al., 2014; Morones et al., 2005). Additionally, the positively charged AgNPs are believed to attach with negatively charged bacterial cell membranes, which lead to rupture of cell wall and disruption of metabolic processes and surface proteins leading to cell death (Sui et al., 2006). Penetration of AgNPs into the bacteria has been reported to inactivate the enzymes and produce H_2O_2 causing cell death (Raffi et al., 2008). Furthermore, Cu-NPs were found to cause multiple toxic effects such as generation of reactive oxygen species, destruction of the cell wall of bacteria, lipid peroxidation, protein oxidation, inhibition of DNA replication and DNA degradation in microorganisms (Chatterjee et al., 2014; Shankar et al., 2014). The obtained results indicated that Ag-Cu NPs are more effective against Gram-negative (*S. typhimurium*) than Gram-positive (*L. monocytogenes*) bacteria. Earlier, a similar behavior has been observed for PLA/Ag-Cu film. It is argued that the microbial inactivation was attributed to the differences in cell wall structures of the microorganisms (Ahmed et al., 2016a; Valodkar et al., 2011).

4. Conclusion

In this study, GG based nanocomposite films were developed by incorporating different levels of Ag-Cu nanoparticles. Properties of the GG films were greatly influenced by the level of NPs reinforced into film forming matrix. A significant improvement in the mechanical properties of the GG NC films achieved by introducing NPs where a uniform distribution of NP was visualized through SEM. Visual color and optical properties of GG films were influenced by the reinforcement of Ag-Cu NPs. The NC films had the excellent barrier property against the light in the UV range. The permeability of the GG films to oxygen significantly dropped with NP loading into the film. Thermal properties of GG films improved with incorporation of NPs. The developed NC films showed excellent antimicrobial activity against *L. monocytogenes* and *S. thyphimurium*. Overall, based on the findings in this work, the GG/Ag-Cu nanocomposite films had potential for development of active packaging to inhibit the growth of microorganisms, extending food shelf-life and ensure food safety. Moreover, it could be used as UV defensive packaging material for UV-sensitive foods to prevent lipid oxidation. Before commercialization of the nanocomposite films, a sincere evaluation of nanoparticle migration to food samples and exposure levels to human health are required to measure which are crucial for such newly developed materials.

Acknowledgments

The authors express their gratitude to the Kuwait Foundation for Advancement of Sciences (KFAS) and the Kuwait Institute for Scientific Research for providing the grant for the research work (Grant number FB 087C).

References

Ahmed, J., Hiremath, N., & Jacob, H. (2016). Antimicrobial efficacies of essential oils/nanoparticles incorporated polylactide films against *L. monocytogenes* and *S. typhimurium* on contaminated cheese. *International Journal of Food Properties*, http://dx.doi.org/10.1080/10942912.2015.1131165

Ahmed, J., Arfat, Y. A., Castro-Aguirre, E., & Auras, R. (2016). Mechanical, structural and thermal properties of Ag-Cu and ZnO reinforced polylactide nanocomposite films. *International Journal of Biological Macromolecules*, *86*, 885–892.

Alamsi, H., Ghanbarzadeh, B., & Entezami, A. A. (2010). Physicochemical properties of starch-CMC-nanoclay biodegradable films. *International Journal of Biological Macromolecules*, *46*, 1–5.

Arfat, Y. A., Benjakul, S., Prodpran, T., & Osako, K. (2014). Development and characterisation of blend films based on fish protein isolate and fish skin gelatin. *Food Hydrocolloids*, *39*, 58–67.

Arfat, Y. A., Benjakul, S., Vongkamjan, K., Sumpavapol, P., & Yarnpakdee, S. (2015). Shelf-life extension of refrigerated sea bass slices wrapped with fish protein isolate/fish skin gelatin-ZnO nanocomposite film incorporated with basil leaf essential oil. *Journal of Food Science and Technology*, *52*, 6182–6193.

Arfat, Y. A., Benjakul, S., Prodpran, T., Sumpavapol, P., & Songtipya, P. (2016). Physico-mechanical characterization and antimicrobial properties of fish protein isolate/fish skin gelatin-zinc oxide (ZnO) nanocomposite films. *Food and Bioprocess Technology*, *9*, 101–112.

Banegas, R. S., Zornio, C. F., Borges, A. D. M., Porto, L. C., & Soldi, V. (2013). Preparation, characterization and properties of films obtained from cross-linked guar gum. *Polímeros*, *23*, 182–188.

Bhattacharya, M., Biswas, S., & Bhowmick, A. K. (2011). Permeation characteristics and modeling of barrier properties of multifunctional rubber nanocomposites. *Polymer*, *52*, 1562–1576.
Cacciotti, I., Fortunati, E., Puglia, D., Kenny, J. M., & Nanni, F. (2014). Effect of silver nanoparticles and cellulose nanocrystals on electrospun poly (lactic) acid mats: Morphology, thermal properties and mechanical behavior. *Carbohydrate Polymers*, *103*, 22–31.
Cerqueira, M. A., Souza, B. W., Teixeira, J. A., & Vicente, A. A. (2012). Effect of glycerol and corn oil on physicochemical properties of polysaccharide films–A comparative study. *Food Hydrocolloids*, *27*, 175–184.
Chatterjee, A. K., Chakraborty, R., & Basu, T. (2014). Mechanism of antibacterial activity of copper nanoparticles. *Nanotechnology*, *25*, 135101.
Coma, V. (2013). Polysaccharide-based biomaterials with antimicrobial and antioxidant properties. *Polímeros*, *23*, 287–297.
Cunha, P. L., Castro, R. R., Rocha, F. A., de Paula, R. C., & Feitosa, J. P. (2005). Low viscosity hydrogel of guar gum: Preparation and physicochemical characterization. *International Journal of Biological Macromolecules*, *37*, 99–104.
Cushen, M., Kerry, J., Morris, M., Cruz-Romero, M., & Cummins, E. (2013). Migration and exposure assessment of silver from a PVC nanocomposite. *Food Chemistry*, *139*(14), 389–397.
Dizaj, S. M., Lotfipour, F., Barzegar-Jalali, M., Zarrintan, M. H., & Adibkia, K. (2014). Antimicrobial activity of the metals and metal oxide nanoparticles. *Materials Science & Engineering C -Materials Today*, *44*, 278–284.
Emamifar, A., Kadivar, M., Shahedi, M., & Soleimanian Zad, S. (2011). Effect of nanocomposite packagingcontaining Ag and ZnO on inactivation of *Lactobacillus plantarum* in orange juice. *Food Control*, *22*, 408–413.
Fringant, C., Tvaroska, I., Mazeau, K., Rinaudo, M., & Desbrieres, J. (1995). Hydration of α-maltose and amylose: Molecular modelling and thermodynamics study. *Carbohydrate Research*, *278*, 27–41.
Gong, H., Liu, M., Zhang, B., Cui, D., Gao, C., Ni, B., et al. (2011). Synthesis of oxidized guar gum by dry method and its application in reactive dye printing. *International Journal of Biological Macromolecules*, *49*, 1083–1091.
Hannon, J. C., Kerry, J., Cruz-Romero, M., Morris, M., & Cummins, E. (2015). Advances and challenges for the use of engineered nanoparticles in food contact materials. *Trends Food Sci. Technol.*, *43*(1), 43–62.
Hannon, J. C., Kerry, J. P., Cruz-Romero, M., Azlin-Hasim, S., Morris, M., & Cummins, E. (2015). An assessment of the migration potential of nanosilver from nanoparticle coated low density polyethylene food packaging into food simulants. *Food Additives & Contaminants: Part A*, *33*(1), 167–178.
Hannon, J. C., Kerry, J. P., Cruz-Romero, M., Azlin-Hasim, S., Morris, M., & Cummins, E. (2016). Human exposure assessment of silver and copper migrating from an antimicrobial nanocoated packaging material into an acidic food simulant. *Food and Chemical Toxicology*, *95*, 128–136.
Jamshidian, M., Tehrany, E. A., Imran, M., Jacquot, M., & Desobry, S. (2010). Poly-lactic acid: Production, applications, nanocomposites, and release studies. *Comprehensive Reviews in Food Science and Food Safety*, *9*, 552–571.
Kačuráková, M., Ebringerova, A., Hirsch, J., & Hromadkova, Z. (1994). Infrared study of arabinoxylans. *Journal of the Science of Food and Agriculture*, *66*, 423–427.
Kačuráková, M., Belton, P. S., Wilson, R. H., Hirsch, J., & Ebringerová, A. (1998). Hydration properties of xylan-type structures: An FTIR study of xylooligosaccharides. *Journal of the Science of Food and Agriculture*, *77*, 38–44.
Kanmani, P., & Rhim, J. W. (2014). Physical, mechanical and antimicrobial properties of gelatin based active nanocomposite films containing AgNPs and nanoclay. *Food Hydrocolloids*, *35*, 644–652.
Krochta, J. M., & De Mulder-Johnston, C. (1997). Edible and biodegradable polymer films: Challenges and opportunities. *Food Technology*, *51*, 61–74.
Kumar, A., De, A., & Mozumdar, S. (2015). Synthesis of acrylate guar-gum for delivery of bio-active molecules. *Bulletin of Materials Science*, *38*, 1025–1032.
Li, W.-R., Xie, X.-B., Shi, Q.-S., Duan, S.-S., Ouyang, Y.-S., & Chen, Y.-B. (2011). Antibacterial effect of silver nanoparticles on Staphylococcus aureus. *Biometals: An International Journal on the Role of Metal Ions in Biology, Biochemistry, and Medicine*, *24*(1), 135–141.
Mbhele, Z. H., Salemane, M. G., van Sittert, C. G. C. E., Nedeljkovic, J. M., Djokovic, V., & Luyt, A. S. (2003). *Chemistry of Materials*, *15*, 5019.
Morones, J. R., Elechiguerra, J. L., Camacho, A., Holt, K., Kouri, J. B., & Ramirez, J. T. (2005). The bactericidal effect of silver nanoparticles. *Nanotechnology*, *16*, 2346–2353.
Mudgil, D., Barak, S., & Khatkar, B. S. (2012). X-ray diffraction, IR spectroscopy and thermal characterization of partially hydrolyzed guar gum. *International Journal of Biological Macromolecules*, *50*, 1035–1039.
Petersson, L., & Oksman, K. (2006). Biopolymer based nanocomposites: Comparing layered silicates and microcrystalline cellulose as nanoreinforcement. *Composites Science and Technology*, *66*, 2187–2196.
Raffi, M., Hussain, F., Bhatti, T. M., Akhter, J. I., Hameed, A., & Hasan, M. M. (2008). Antibacterial characterization of silver nanoparticles against *E coli* ATCC 15224. *Journal of Materials Science and Technology*, *24*, 192–196.
Ramos-Sanchez, M. C., Rey, F. J., Rodriguez, M. L., Martin-Gil, F. J., & Martin-Gil, J. (1988). *Thermochimica Acta*, *134*, 55–60.
Rhim, J. W., & Ng, P. K. (2007). Natural biopolymer-based nanocomposite films for packaging applications. *Critical Reviews in Food Science and Nutrition*, *47*, 411–433.
Rhim, J. W., Wang, L. F., & Hong, S. I. (2013). Preparation and characterization of agar/silver nanoparticles composite films with antimicrobial activity. *Food Hydrocolloids*, *33*, 327–335.
Rouhi, J., Mahmud, S., Naderi, N., Ooi, C. H. R., & Mahmood, M. R. (2013). Physical properties of fish gelatin-based bio-nanocomposite films incorporated with ZnO nanorods. *Nanoscale Research Letters*, *8*, 364–370.
Saberi, B., Thakur, R., Vuong, Q. V., Chockchaisawasdee, S., Golding, J. B., Scarlett, C. J., et al. (2016). Optimization of physical and optical properties of biodegradable edible films based on pea starch and guar gum. *Industrial Crops and Products*, *86*, 342–352.
Saurabh, C. K., Gupta, S., Bahadur, J., Mazumder, S., Variyar, P. S., & Sharma, A. (2015). Mechanical and barrier properties of guar gum based nano-composite films. *Carbohydrate Polymers*, *124*, 77–84.
Saurabh, C. K., Gupta, S., Variyar, P. S., & Sharma, A. (2016). Effect of addition of nanoclay, beeswax, tween-80 and glycerol on physicochemical properties of guar gum films. *Industrial Crops and Products*, *89*, 109–118.
Shankar, S., Teng, X., & Rhim, J. W. (2014). Properties and characterization of gelatin/CuNP bionanocomposite films prepared with different copper salts and reducing agents. *Carbohydrate Polymers*, *114*, 484–492.
Shankar, S., Teng, X., Li, G., & Rhim, J. W. (2015). Preparation, characterization, and antimicrobial activity of gelatin/ZnO nanocomposite films. *Food Hydrocolloids*, *45*, 264–271.
Steel, R. G. D., & Torrie, J. H. (1980). *Principle and procedure of statistics* (2nd ed.). New York: McGraw-Hill.
Sui, Z. M., Chen, X., Wang, L. Y., Xu, L. M., Zhuang, W. C., Chai, Y. C., et al. (2006). Capping effect of CTAB on positively charged Ag nanoparticles. *Physica E*, *33*, 308–314.
Tan, K. S., & Cheong, K. Y. (2013). Advances of Ag, Cu, and Ag-Cu alloy nanoparticles synthesized via chemical reduction route. *Journal of Nanoparticle Research*, *15*, 4.
Taner, M., Sayar, N., Yulug, I. G., & Suzer, S. (2011). Synthesis, characterization and antibacterial investigation of silver-copper nanoalloys. *Journal of Materials Chemistry*, *21*, 13150–13154.
Teixeira, B., Marques, A., Pires, C., Ramos, C., Batista, I., Saraiva, J. A., et al. (2014). Characterization of fish protein films incorporated with essential oils of clove, garlic and origanum Physical, antioxidant and antibacterial properties. *LWT–Food Science and Technology*, *59*, 533–539.
Valodkar, M., Modi, S., Pal, A., & Thakore, S. (2011). Synthesis and anti-bacterial activity of Cu, Ag and Cu-Ag alloy nanoparticles: A green approach. *Materials Research Bulletin*, *46*, 384–389.
Varshney, R., Bhadauria, S., Gaur, M. S., & Pasricha, R. (2010). Characterization of copper nanoparticles synthesized by a novel microbiological method. *JOM*, *62*, 102–104.
Vroman, I., & Tighzert, L. (2009). Biodegradable polymers. *Materials*, *2*, 307–344.
Zain, N. M., Stapley, A. G. F., & Shama, G. (2014). Green synthesis of silver and copper nanoparticles using ascorbic acid and chitosan for antimicrobial applications. *Carbohydrate Polymers*, *112*, 195–202.
Zeng, R., Rong, M. Z., Zhang, M. Q., Lianm, H. C., & Zeng, H. M. (2001). Interfacial interaction in Ag/polymer nanocomposite films. *Journal of Materials Science Letters*, *20*, 1473–1476.
de Moura, M. R., Aouada, F. A., Avena-Bustillos, R. J., McHugh, T. H., Krochta, J. M., & Mattoso, L. H. (2009). Improved barrier and mechanical properties of novel hydroxypropyl methylcellulose edible films with chitosan/tripolyphosphate nanoparticles. *Journal of Food Engineering*, *92*, 448–453.